Electronic Structure of Mono- and Bis(carbonyliron) as well as Bis(cyclopentadienyliron) Complexes of 1,4-Dihydro-1,4-diboranaphthalene

Rolf Gleiter*[a], Isabella Hyla-Kryspin[a], and Walter Siebert[b]

Organisch Chemisches Institut[a] und Anorganisch Chemisches Institut[b] der Universität Heidelberg, Im Neuenheimer Feld 270, D-69120 Heidelberg, Germany

Received January 17, 1994

Key Words: MO calculations, EH / Iron, tricarbonyl(η^6-1,4-dihydro-1,4-diboranaphthalene)- / Bis(tricarbonyliron) / Dicarbonyliron-tricarbonyliron / Bis(cyclopentadienyliron) complexes

The structure and bonding of four iron complexes involving the 1,4-dihydro-1,4-diboranaphthalene ligand $C_8B_2H_8$ (**1**), namely of the complexes $(CO)_3Fe(\eta^6\text{-}C_8B_2H_8)$ (**2**), $(\mu,\eta^4,\eta^6\text{-}C_8B_2H_8)[Fe(CO)_3]_2$ (**3**), $(CO)_3Fe(\mu,\eta^4,\eta^6\text{-}C_8B_2H_8)Fe(CO)_2$ (**4**), and of the triple-decker $(\mu\text{-},\eta^6\text{-}C_8B_2H_8)[Fe(\eta^5\text{-}C_5H_5)]_2$ (**5**), have been investigated by means of the perturbational molecular orbital theory on the basis of the Extended Hückel calculations. Compounds **2** and **3** are 18-VE complexes, whereas **5** is a 30-VE species. The structure of **4** can be best described in terms of a 16-VE complex "$Fe(CO)_3$ · heterocycle" and a 18-VE "$Fe(CO)_2$ · carbocycle" unit with its iron centers being not directly bond.

2,3-Diethyl-1,4-dihydro-1,4-dimethyl-1,4-diboranaphthalene (**1**, R^1 = Et, R^2 = Me)[1] exhibits unique ligand properties toward metal complex fragments. Reactions of **1** with $(CO)_3Fe(C_8H_{14})_2$ lead to the red complex **2** (R^1 = Et, R^2 = Me)[2] and to the orange *anti*-dinuclear complex **3** as well as to the cherry-red *syn* complex **4**[3]. At higher temperature **1** reacts with $[(C_5H_5)Fe(C_8H_{12})]_2Zn$ to give the diamagnetic 30-VE triple-decker sandwich **5**[3]. Several nickel complexes[4] have been obtained from **1** and $Ni(C_8H_{12})_2$, $Ni(C_3H_5)_2$, or $[BrNi(C_3H_5)]_2$. It is assumed that in the reaction of **1** with $(CO)_3Fe(C_8H_{14})_2$ the 16-VE fragment $[(CO)_3Fe(C_8H_{14})]$ is first η^2-coordinated to the double bond of the heterocycle to yield the intermediate $[(CO)_3Fe(C_8H_{14})(\mathbf{1})]$, which loses C_8H_{14} to give the structurally characterized tricarbonyliron complex **2**. The η^6 coordination causes a severe perturbation of the aromatic benzo ring, and the formed diene **2** may be attacked in *anti* or *syn* position by a second $(CO)_3Fe$ unit to form **3** or **4**, respectively. The 13-VE fragment $[(C_5H_5)Fe]$ and **1** yield the unstable, 17-VE sandwich intermediate $(C_5H_5)Fe(\mathbf{1})$, which is stacked to give the 30-VE triple-decker **5**. In this paper we report on calculations to elucidate the electronic structures of the four complexes **2**–**5** (R^1 = R^2 = H).

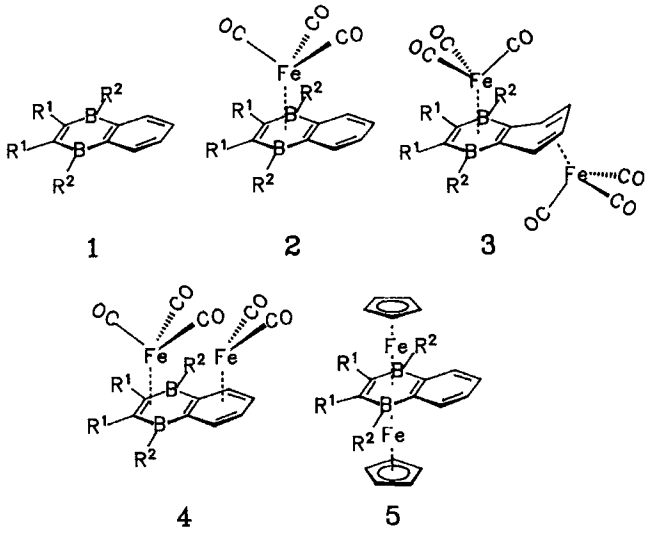

Electronic Structure and Bonding

To obtain an insight into the electronic structure of **2**–**5** (R^1 = R^2 = H) we adopt Hoffmann's fragment MO approach and make use of a perturbational analysis based on Extended Hückel (EH) calculations[5,6]. According to X-ray data, complex **3** (R^1 = Et, R^2 = Me) has C_s symmetry[3]. In the case of **2** and **4** we adopt the slightly idealized C_s symmetry (mirror plane *yz*); the symmetry of **5** is assumed to be C_{2v}.

The geometrical parameters of the free $C_8B_2H_8$ ligand are approximated on the basis of the experimental structure of 9,10-dihydro-9,10-dimethyl-9,10-diboraanthracene[7]. The parameters used in the EH calculations as well as the most important geometrical parameters of **1**–**5** are given in the Appendix. Firstly, we examine the electronic structure of **2**. We will focus on the shapes and energies of its frontier orbitals, since they will play a crucial role in the bonding of the second metal complex fragment. We continue with an analysis of the bonding in **3** and **4**, and we discuss the factors responsible for its stabilization and geometrical structure. Finally, we describe the electronic structure of **5**.

Mononuclear Complex 2

Compound **2** can be viewed as being composed of two fragments: $C_8B_2H_8$ and $Fe(CO)_3$. Figure 1 shows a simpli-

  0009–2940/94/0909–1557 $ 10.00+.25/0

fied interaction diagram, displaying only those frontier orbitals of the two units which are mainly involved in the bonding interactions with each other. The frontier orbitals of the $Fe(CO)_3$ unit are well-known[5]. On the left side of Figure 1 we show only the set of three valence hybrid orbitals (1a″, 1a′, 2a′) containing a total of two electrons which can participate in the backdonation from the metal to the ligand. We have omitted three occupied orbitals, originating from the "t_{2g}" set of the octahedron. The frontier orbitals of the ligand **1** are shown on the right side of Figure 1.

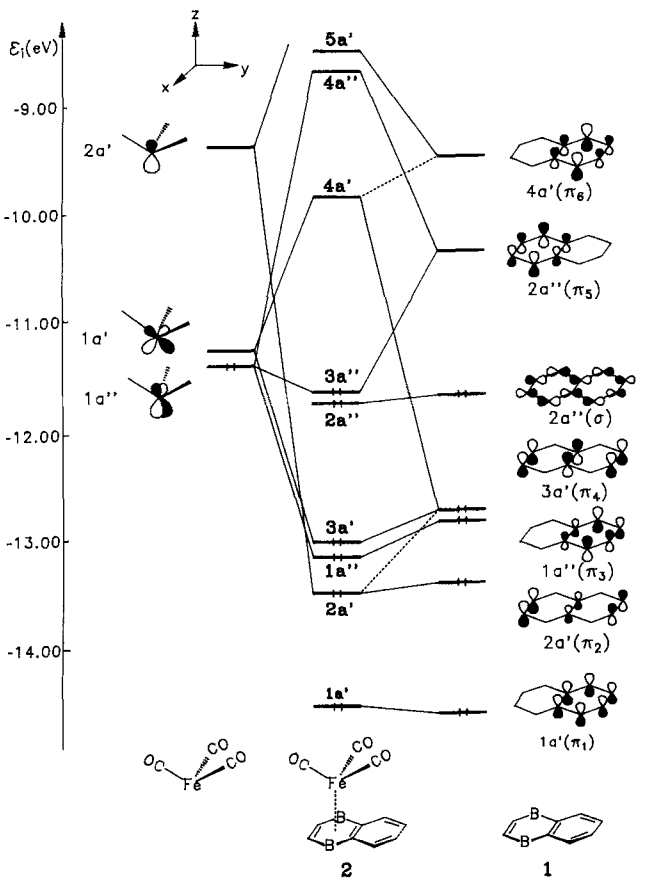

Figure 1. Simplified interaction diagram for the interaction between the $Fe(CO)_3$ unit and $C_8B_2H_8$ to give **2**

For the sake of clarity we have omitted some levels that describe the C–C σ bonds and do not participate in the bonding with the metal fragment. It is noted, that the HOMO of **1** has σ character. An examination of the p_z components in the π MOs of **1** points to an uneven distribution of the π electron density among the π levels. In the 1a′ (π_1) and 1a″ (π_3) MOs the π electron density is localized on the carbocycle of **1** whereas in 2a′ (π_2) and 3a′ (π_4) it is delocalized over both cycles of **1**. An uneven distribution of the π electron density will obviously influence the preferential coordination site of the metal fragment to the ligand. The low-lying LUMO 2a″ (π_5) is localized on the heterocycle of **1**, and to achieve strong backbonding from the frontier metal orbital 1a″, the $Fe(CO)_3$ unit coordinates to the heterocycle of **1**. As a result one obtains the bonding HOMO 3a″ and the empty 4a″ level of **2**. We notice a strong interaction of the orbitals of a′ symmetry, i.e. 1a′ of the metal fragment with 2a′(π_2), 3a′(π_4), and 4a′(π_6) of the ligand. As a result of this interaction a considerable mixing of the wave functions is found. The resulting wave functions can be derived by applying the rules of the second-order perturbation theory[5,8]. The result is shown on the left side of Figures 2 and 5 (broken boxes).

Dinuclear *trans* Complex 3

The dinuclear complex **3** can be analyzed in a similar manner. To obtain more information about its electronic structure we examine first the bonding in three isomers **3a–c**, all being composed of the complex **2a**, the rotamer of complex **2**, and a second $Fe(CO)_3$ unit. We notice that the shapes of the valence MOs of **2a** do not much differ from those of **2**, however, the bonding interactions in **2** are stronger than in **2a**. The rotamer **2a** is by 5 kcal/mol less stable than complex **2**. In **3a** and **3b** the second $Fe(CO)_3$ unit coordinates in an η^6 manner to the hetero- and carbocycle of **2**, respectively. In **3c** it binds in a η^4 manner to the carbocycle.

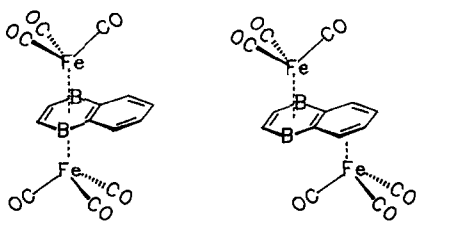

A simplified interaction diagram in the case of **3b** is shown in Figure 2. On the left side of Figure 2 we have omitted the 2a″ level of **2a** (cf. Figure 1) describing the highest σ orbital of **1**. From the localization of the wave functions it follows for **3b** that 2a′ and 3a″ will not contribute to the bonding with a second $Fe(CO)_3$ unit. However, there is a good matching between the 1a″ levels of both fragments. It results in a lower energy, an occupied 1a″ MO and the LUMO 4a″ of **3b**. In this case, the two cylindrical MOs of both units, 1a′ of **2a** and 2a′ of $Fe(CO)_3$, interact with each other, giving the low-energy occupied 1a′ MO and at high energy an empty level of **3b**. To derive the wave functions of the orbitals belonging to the irreducible representation A′ from those of **2a** and another $Fe(CO)_3$ unit we can again use the second-order perturbation theory. The mixing of 3a′, 4a′ of **2a** with 1a′ of $Fe(CO)_3$ gives rise to 2a′, 4a′, and 5a′ (the latter not shown in Figure 2) of **3b**. The wave functions 2a′ and 4a′ are shown in Figure 3.

While 2a′ retains essentially the shape of 3a′ with the anticipated bonding admixture of 1a′ of the metal fragments, 4a′ changes its character considerably. The still antibonding character of the HOMO 4a′ of **3b** can be changed to a bonding one by a geometrical perturbation. A simplified Walsh diagram as well as the relative energies (E_{rel}) and reduced overlap populations (ROVP) are presented in Figure 4. The electronic structures of **3a** and **3b** are comparable to that of the paramagnetic 32-VE complex [(η^5-

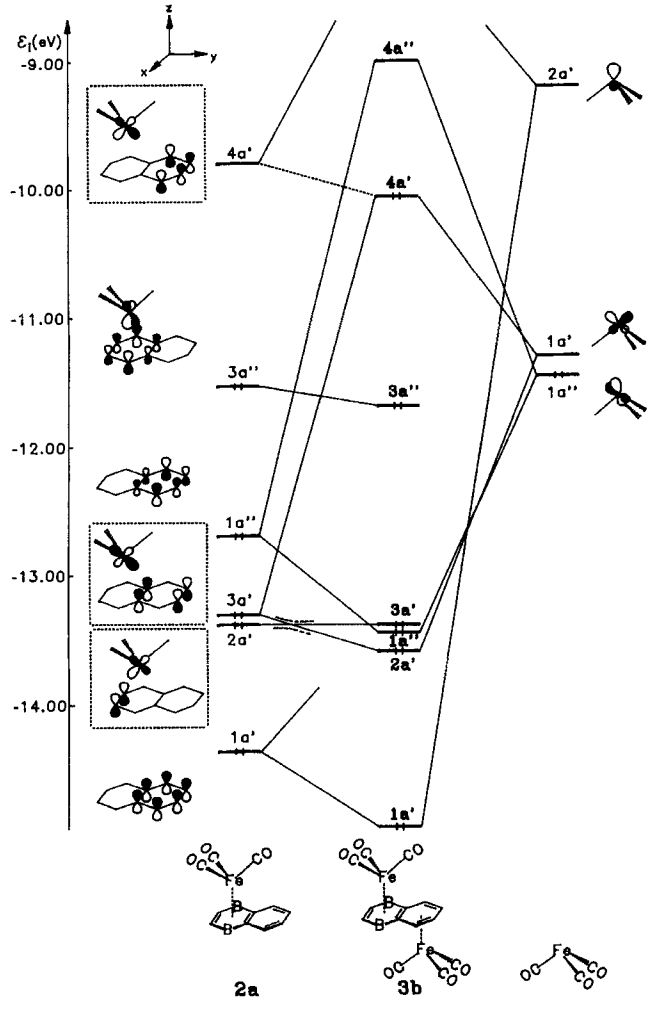

Figure 2. Simplified interaction diagram for the interactions of complex **2a** with the second $Fe(CO)_3$ unit to give **3b**

$C_5H_5)Co]_2[\mu,\eta^6,\eta^6\text{-}(EtC)_2\ (MeB)_2(CH)_2]$[9]. However, the two valence electrons in **3a** and **3b** are located in antibonding levels. The shift of the $Fe(CO)_3$ unit to an η^4 coordination to give **3c** stabilizes the HOMO and destabilizes the 2a′ level. The folding of the carbocycle along the vector C7–C10 to give **3** transforms the HOMO to a perfect bonding level and changes the 2a′ level to the nonbonding one. As a consequence of the character of the HOMO the calculations predict that **3** is by 64.3, 56.4, and 28.6 kcal/mol more stable than **3a**, **3b**, and **3c**, respectively. In the case of **3** four donating electrons are stabilized on the 1a′ and 1a″ levels, and two electrons are involved in the backbonding on the HOMO 4a′. Together with the six electrons from the "t^6_{2g}"-like metal levels of the second metal complex fragment and the six electrons involved in iron-carbonyl σ bonds, it yields a total of 18 VE. Thus, the complex **3** can be considered as a 36-VE species, composed of two 18-VE units.

Dinuclear Complex 4

In the complex **4** both metal fragments are bound to the same side of ligand **1**. The $Fe(CO)_3$ unit coordinates in an η^4 manner to the heterocycle and the $Fe(CO)_2$ unit in an η^6 manner to the carbocycle of the ligand **1**. Thus, a convenient way to examine the bonding in **4** is to build up this molecule from the "distorted complex" **2b** and a $Fe(CO)_2$ unit. In **2b** the $Fe(CO)_3$ unit is moved by ≈ 0.34 Å from the middle of the heterocycle towards the double bond. On the left side of Figure 5 we show the MOs of **2b**, a slightly distorted structure of **2**. As anticipated, this distortion leads to a stabilization of MO 2a′ and a destabilization of 3a′ and 1a″ as compared to the corresponding MOs of **2** (see Figure 1). The empty 4a′ MO of **2** which is antibonding is stabilized in **2b** to be nonbonding. The valence MOs of $Fe(CO)_2$ are shown on the right side of Figure 5. They can be easily derived from those of $Fe(CO)_3$. Removal of one carbonyl from $Fe(CO)_3$ stabilizes the 1a′ level, all other MOs remaining unaffected.

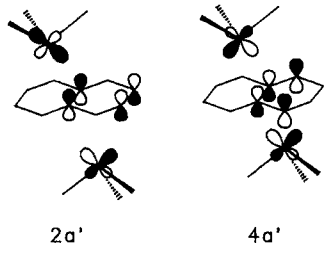

Figure 3. Schematic representation of 2a′ and 4a′ of **3b**

Two MOs 2a′ and 3a″ of **2b** do not participate in the bonding with $Fe(CO)_2$. In this case, there is a good matching between occupied and empty levels of both fragments. The 1a′ and 1a″ levels of **2b** are stabilized each by two-electron, two-orbital interactions with the empty 2a′ and 1a″ MOs of $Fe(CO)_2$, respectively. The MOs 3a′ and 4a′ of **2b** interact with 1a′ of $Fe(CO)_2$. This gives rise to a bonding orbital (2a′), a nonbonding HOMO (4a′), and the antibonding LUMO (5a′). The calculated HOMO-LUMO gap (1.7 eV) is large enough to predict a singlet ground state for **4**. Eight electrons are stabilized in those interactions. Together with ten remaining electrons of $Fe(CO)_2$ (6e from "t^6_{2g}"-like levels and 4e involved in iron-carbonyl σ bonds) this yields a total of 18 VE for the "$Fe(CO)_2$-carbocycle" unit of **4**. Thus, complex **4** can be considered as a 34-VE molecule, composed of the 16-VE "$Fe(CO)_3$ · heterocycle" and the 18-VE "$Fe(CO)_2$ · carbocycle" units.

There are also two other possibilities of constructing complex **4** from 16-VE and 18-VE units as shown in **4a** and **4b**.

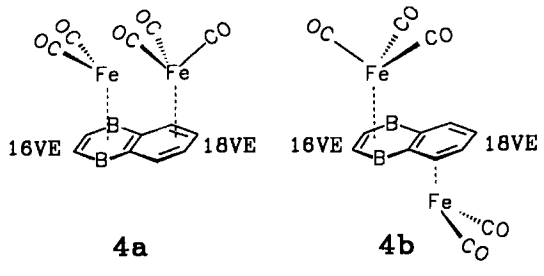

The EH calculations using standard parameters predict that **4** and **4b** have a comparable energy while **4a** is by 12

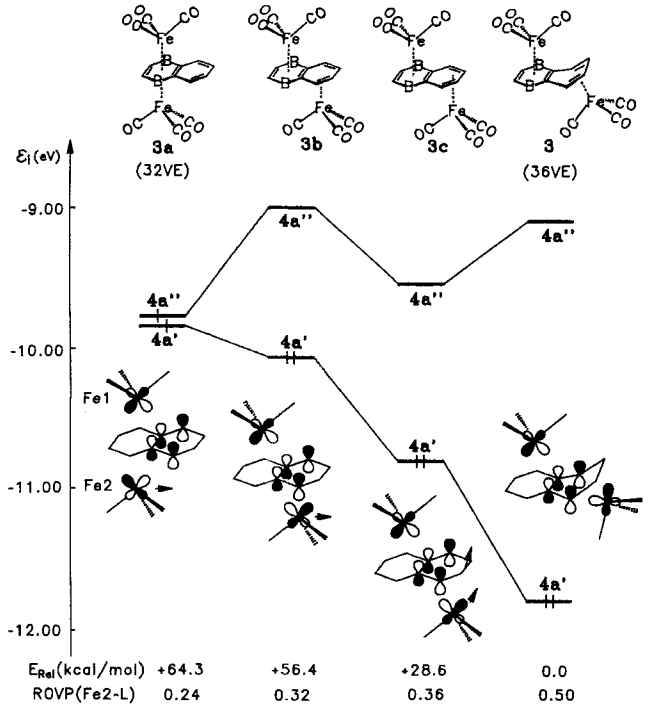

Figure 4. Simplified Walsh diagram for the geometrical distortion in **3**

kcal/mol less stable than **4**. The reason why **4** is favoured by experiment with respect to **4a** and **4b** is not clear-cut. The interactions between the t_{2g}-like MOs of both Fe atoms give no contribution to the stabilization. The resulting MO wave functions are characterized as three bonding and three antibonding combinations of the t_{2g}-like levels of the Fe atoms. However, in **4a** the HOMO-LUMO gap is relatively small (1.1 eV), suggesting a triplet ground state with one electron in the antibonding 5a′ level. A comparison of the most relevant wave functions of the three species in question shows that in **4** an Fe–Fe σ-orbital contributes to the stabilization which exhibits an Fe–Fe bonding character as shown in **A**. Although the metal character of this MO amounts only to 27%, its antibonding counterpart is not occupied. This MO obviously is absent in **4b**.

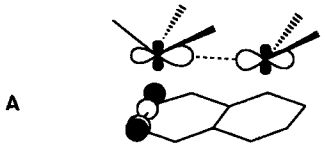

Extended Hückel calculations with charge iterations on the iron atoms predict that **4b** is by 25 kcal/mol less stable than **4**. However, a detailed analysis of the stabilizing interactions prevailing in **4**, **4a**, and **4b** requires a full geometry optimization for all isomers. Extended Hückel calculations are not well suited to reach this goal.

Triple-Decker Complex 5

A convenient way to analyze the bonding in the triple-decker **5** is to build it from the FeCp dimer (**6**) and the $C_8B_2H_8$ ligand. A simplified interaction diagram is shown in Figure 6. The frontier orbitals of the MCp dimer are

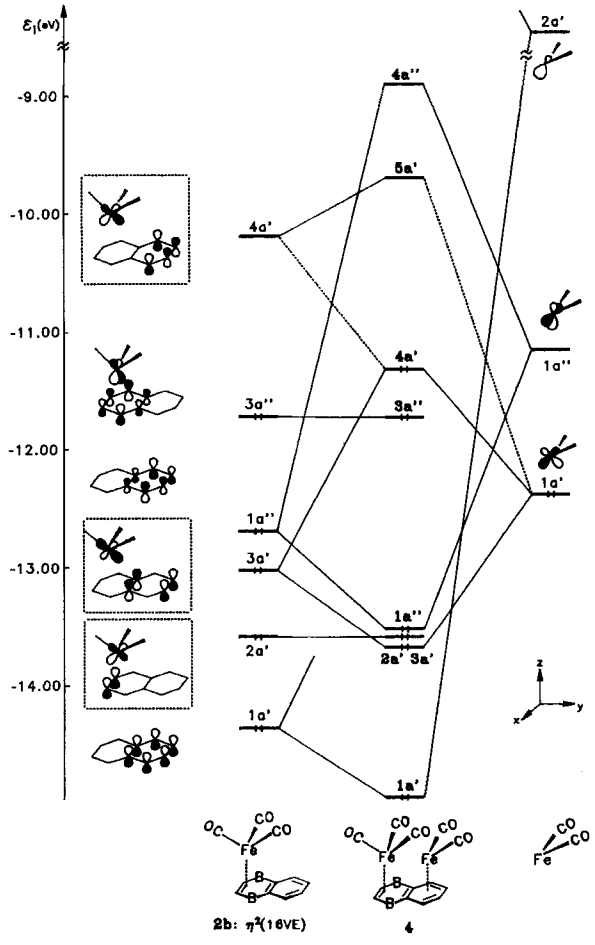

Figure 5. Simplified interaction diagram for the interactions of $Fe(CO)_3(C_8B_2H_8)$ (**2a**) with the $Fe(CO)_2$ unit

well-known[5,10], they are shown on the left side of Figure 6. Although the local symmetry of the FeCp dimer is D_{5h}, we label its frontier MOs according to C_{2v}, the symmetry of complex **5**. For the sake of clarity we have omitted in Figure 6 the six occupied MOs describing the Fe–Cp bonding as well as six metal-centered levels, all being left nonbonding with respect to the ligand **1**. The four nearly degenerated valence MOs of **6** ($1a_1$, $1b_1$, $1b_2$, $1a_2$) contain a total of two electrons that can participate in the backdonation from the metals to the bridging ligand. They are followed by two high-lying empty levels $2a_1$ (omitted in Figure 6) and $2b_2$ (Figure 6).

Three of the above-mentioned levels ($1a_1$, $1b_1$, $2a_1$) are left nonbonding with respect to the ligand **1**. The frontier MOs of ligand **1** are shown on the right side of Figure 6. In this case there is a good matching between occupied and empty orbitals of both units. $1b_2$ of **6** interacts with $3b_2$ (π_4) of **1** giving the low-lying occupied $3b_2$ MO and the LUMO $4b_2$ of **5**, while $1a_2$ of **6** interacts with $2a_2$ (π_5) of **1**, giving the occupied $2a_2$ MO and the empty $3a_2$ level of **5**. Similarly, as in the case of **2**, the $2b_2$ (π_2) MO of **1** has a proper local symmetry to interact with the high-lying $2b_2$ MO of **6**. The result is a low-energy occupied $2b_2$ MO and an empty high-lying level of **5**. As in the case of **2**, the second-order mixing between $3b_2$ (π_4) and $2b_2$ (π_2) MOs of

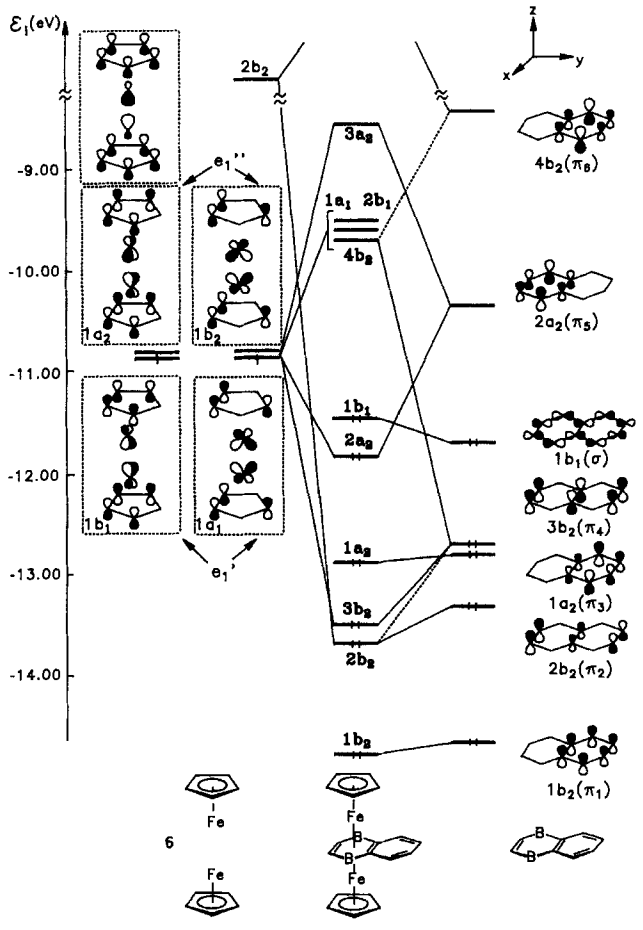

Figure 6. Simplified interaction diagram for the interactions of the $Fe(C_5H_5)$ dimer (**6**) with the $C_8B_2H_8$ ligand

1 via the metal-localized $1b_2$ (yz) level of **6** supports the stabilization of the $2b_2$ MO of **5**. It is clear, that the carbocycle-localized MOs of **1**, $1b_2$ (π_1) and $1a_2$ (π_3), do not participate in the bonding. Four donating electrons of **1** are stabilized on the $2b_2$ and $3b_2$ levels of **5**. Two electrons participate in the backbonding in the $2a_2$ MO. Together with 24 electrons from the remaining nonbonding orbitals of **6**, this yields a total of 30 VE, which correspond to a stable situation equivalent to other 30-VE triple-deckers[10]. We conclude, that the stabilizing interactions present in the 18-VE complex **2** and 30-VE complex **5** have entirely the same character.

We are grateful to the *Deutsche Forschungsgemeinschaft* (SFB 247) and the *Fonds der Chemischen Industrie* for financial support.

Appendix

The calculations were carried out using the Extended Hückel method[6a,b] with parameters as listed in Table 1. A modified Wolfsberg-Helmholz formula[6e] was used throughout the calculations. In the calculations with charge iterations, the VSIE (q) functions for iron s, p, and d orbitals were assumed to be of the form VSIE (q)=$Aq^2 + Bq + C$. We have used nine A, B, and C parameters from Ref.[6f].

Table 1. Extended-Hückel parameters

	Orb.	*H*ii (eV)	ξ_1	ξ_2[a]	c_1[a]	c_2[a]	Ref.
H	1 s	−13.60	1.30				[6b]
B	2 s	−15.20	1.30				[6c]
	2 p	−8.20	1.30				
C	2 s	−21.40	1.625				[6b]
	2 p	−11.40	1.625				
O	2 s	−32.30	2.275				[6b]
	2 p	−14.80	2.275				
Fe	4 s	−9.10	1.90				[6d]
	4 p	−5.32	1.90				
	3 d	−12.60	5.35	2.00	0.5505	0.6260	

[a] Contraction coefficients in the double ξ expansion.

The geometrical parameters used for the calculations are as follows: Chosen distances [Å] and angles [°]: **1**: B1–C2 1.569; C2–C3 1.418; C6–C7 1.400; C7–C8 1.386; C8–C9 1.366; C2B1C6 118.5; B1C2C3 120.7; C5C6C7 118.2; C6C7C8 122.0; C7C8C9 119.8. Fe1–B1: 2.298 (**2**); 2.311 (**3**); 2.389 (**4**); 2.215 (**5**). Fe1–C2: 2.214 (**2**); 2.221 (**3**); 2.182 (**4**); 2.174 (**5**). Fe1–C5: 2.352 (**2**); 2.335 (**3**); 2.560 (**4**); 2.174 (**5**). Fe2–C5: 2.920 (**3**); 2.188 (**4**). Fe2–C7: 2.172 (**3**); 2.124 (**4**). Fe2–C8: 2.066 (**3**); 2.122 (**4**). Fe–C(CO) = 1.80; Fe–C(Cp) = 2.032; C–O=1.14. – In the case of **3** the torsional angle C8C7C6B1 amounts to 146.5°.

[1] W. Siebert, *Adv. Organomet. Chem.* **1993**, *35*, 187.
[2] A. Feßenbecker, H. Schulz, H. Pritzkow, W. Siebert, *Chem. Ber.* **1990**, *123*, 2273.
[3] H. Schulz, H. Pritzkow, W. Siebert, *Chem. Ber.* **1992**, *125*, 987.
[4] H. Schulz, H. Pritzkow, W. Siebert, *Chem. Ber.* **1992**, *125*, 993.
[5] T. A. Albright, J. K. Burdett, M.-H. Whangbo in *Orbital Interaction in Chemistry*, Whiley, New York, **1985**.
[6] [6a] R. Hoffmann, W. N. Lipscomb, *J. Chem. Phys.* **1962**, *36*, 2179. – [6b] R. Hoffmann, *J. Chem. Phys.* **1963**, *39*, 1397. – [6c] A. B. Anderson, R. Hoffmann, *J. Chem. Phys.* **1974**, *60*, 4271. – [6d] R. H. Summerville, R. Hoffmann, *J. Am. Chem. Soc.* **1976**, *98*, 7240. – [6e] J. H. Ammeter, H.-B. Bürgi, J. C. Thibeault, R. Hoffmann, *J. Am. Chem. Soc.* **1978**, *100*, 3686. – [6f] C. J. Ballhausen, H. B. Gray, *Molecular Orbital Theory*, W. A. Benjamin, Inc. New York, **1965**, p. 125.
[7] P. Müller, Diploma Thesis, University of Heidelberg, **1991**.
[8] [8a] A. Imamura, *Mol. Phys.* **1968**, *15*, 225. – [8b] L. Libit, R. Hoffmann, *J. Am. Chem. Soc.* **1974**, *96*, 1370. – [8c] M.-H. Whangbo, H. B. Schlegel, S. Wolfe, *J. Am. Chem. Soc.* **1977**, *99*, 1296.
[9] W. Siebert, J.-K. Uhm, unpublished.
[10] [10a] J. W. Lauher, M. Elian, H. Summerville, R. Hoffmann, *J. Am. Chem. Soc.* **1976**, *98*, 3219. – [10b] R. Gleiter, I. Hyla-Kryspin, G. E. Herberich, *J. Organomet. Chem.*, in press. – [10c] I. Hyla-Kryspin, R. Gleiter, G. E. Herberich, M. Bénard, *Organometallics*, in press. – [10d] J. Edwin, M. Bochmann, M. C. Böhm, D. E. Brennan, W. E. Geiger, C. Krüger, J. Pebler, H. Pritzkow, W. Siebert, W. Swiridoff, H. Wadepohl, J. Weiss, U. Zenneck, *J. Am. Chem. Soc.* **1983**, *105*, 2582.

[18/94]